Int. J. Heat Mass Transfer. Vol. 24, No. 10, pp. 1699–1710, 1981
Printed in Great Britain

0017 9310/81/101699 12 $02.00/0

HEAT TRANSFER COEFFICIENTS FOR MELTING ABOUT A VERTICAL CYLINDER WITH OR WITHOUT SUBCOOLING AND FOR OPEN OR CLOSED CONTAINMENT

R. G. KEMINK and E. M. SPARROW
Department of Mechanical Engineering, University of Minnesota, Minneapolis, MN 55455, U.S.A.

(*Received* 9 *February* 1981 *and in revised form* 16 *April* 1981)

Abstract—Experiments were undertaken to measure heat transfer coefficients for melting about a heated vertical cylinder embedded in a solid phase-change medium whose temperature was either at the melting point or was subcooled below the melting value. In the experiments, the upper surface of the phase-change medium was either closed by a cover which imposes a no-slip velocity boundary condition on the liquid melt or was bounded by an insulated air space which permits unrestrained motion of the liquid. The shape of the melt region was also measured. All the experiments were performed using 99% pure *n*-eicosane paraffin (melting temperature = 36.4°C) and encompassed both transient and steady-state periods. The cylinder height-to-diameter ratio was ten. It was found that the heat transfer coefficients are identical for the closed-top and open-top configurations. Subcooling tends to delay the onset of natural-convection dominance of the heat transfer process. The natural convection heat transfer coefficients in the presence of subcooling are about 10–15% lower than those for the non-subcooled case. In general, the steady-state natural convection heat transfer coefficients were well correlated in terms of the Nusselt and Rayleigh numbers and, in the absence of subcooling, the functional dependence was shown to be similar to that for natural convection in vertical, parallel walled enclosures without melting.

NOMENCLATURE

A, cylinder surface area;
AR, aspect ratio, L/L^*;
c_p, specific heat;
E, energy input to phase-change medium between $t = 0$ and $t = t$;
g, acceleration of gravity;
h, spatial-average heat transfer coefficient, $Q/A(\bar{T}_w - T^*)$;
k, thermal conductivity;
L, cylinder length;
L_c, characteristic length;
L^*, thickness of effective cross-section;
Nu, Nusselt number, equation (4);
Nu_L, Nusselt number based on L;
Nu_{L^*}, Nusselt number based on L^*;
P, rate of electric power input;
Q, instantaneous rate of heat transfer to phase-change medium;
Ra, Rayleigh number, equation (4);
Ra_L, Rayleigh number based on L;
Ra_{L^*}, Rayleigh number based on L^*;
r_0, radius of cylinder surface;
r^*, outer radius of effective cross section;
S, rate of energy storage in cylinder wall;
x, axial coordinate measured downward from top of cylinder;
$\bar{T}_w$, spatial-average surface temperature of cylinder;
T^*, melting temperature;
t, time.

Greek symbols

β, coefficient of thermal expansion;
λ, latent heat of melting per unit mass;
μ, viscosity;
ν, kinematic viscosity;
ρ, density;
τ, dimensionless time, $E/\rho\lambda\pi r_0^2 L$.

INTRODUCTION

APPLICATIONS to the storage of thermal energy by liquid–solid phase change have evoked a renewed interest in the heat transfer processes which are involved in freezing and melting [1]. It has been demonstrated experimentally that natural convection in the liquid phase can play a dominant role in both freezing and melting. In particular, natural convection in the unfrozen liquid tends to diminish the rate of freezing compared with that which would occur if heat conduction were the sole mode of energy tranport. In the case of melting, the presence of natural convection in the liquid melt increases the rate at which melting takes place.

With the establishment of the qualitative nature of the heat transfer processes that govern freezing and melting (see [1] for a survey of recent literature), the essential task of providing quantitative heat transfer data must be addressed. For melting, which is the focus of this paper, only for the case of the horizontal cylinder is there now available quantitative data suitable for design. For melting adjacent to vertical surfaces, which was studied experimentally in [2–6], heat transfer coefficients were not measured in [2–4], while a limited, exploratory set of results is presented in [5]. Reference [6], at first impression, appears to convey a potentially useful Nusselt number cor-

relation, but careful examination shows that one of the temperatures that appears in the definition of the heat transfer coefficient is, from the standpoint of a user, unknown. Furthermore, both [5] and [6] deal with geometrical configurations that are different from that studied here.

Analytical predictions for melting about a vertical cylinder, with account being taken of natural convection, have been made in [7] and [8], with the latter, in effect, superceding the former. The predicted results cover a narrow parameter range, as will be elaborated later, during the presentation of results.

In the present research, experiments were undertaken to provide quantitative heat transfer information for melting about a heated vertical cylinder embedded in a solid phase-change medium. The work encompassed a broad range of operating conditions. In one set of experiments, the solid was at its melting temperature prior to the onset of the melting process, while in a second set of experiments the solid was at a temperature below the melting point (i.e. subcooled initial condition). For each of these solid-phase thermal conditions, two different containment conditions were investigated. In one of these, the experiments were carried out in an open-topped containment vessel, which allows the liquid melt to flow without any constraint along its upper surface. This absence of a velocity constraint at the upper bounding surface of the containment vessel will be referred to as the slip boundary condition. Experiments were also performed in a closed-topped containment vessel which inhibits the motion of the liquid melt along its upper surface, i.e. a no-slip boundary condition. In the closed-top case, special provisions were required to accommodate the increase in the volume of the melting phase-change material.

For each of the operating conditions, experiments were performed for a range of heat flux densities at the heated cylinder. The phase-change medium used in the experiments is 99% pure *n*-eicosane paraffin, with a measured melting temperature of 36.4°C.

The main objective of the research was to measure and to correlate heat transfer coefficients for the various operating conditions described in the foregoing paragraphs. Results are presented both for the timewise variation of the heat transfer coefficient that accompanies the growth of the melt layer and for the steady-state coefficients that are encountered at large times. The latter are correlated in terms of a Nusselt–Rayleigh relationship and are compared with literature information for natural convection heat transfer (without phase change) in enclosed vertical spaces. Definitive conclusions will be sought about the effects of the initial thermal state of the solid and of the slip vs no-slip velocity boundary condition at the upper surface of the liquid melt. Melt layer shapes were also measured, and these provide clear evidence as to the nature of the energy transport in the liquid melt.

As a supplement to the laboratory work, numerical finite-difference solutions were undertaken to provide perspective for certain of the experimental results.

THE EXPERIMENTS

In the experiments, an electrically heated vertical cylinder was positioned along the axis of a cylindrical containment vessel which housed the phase-change medium. In turn, the vessel was situated in a constant-temperature water bath which served to provide a controlled thermal environment for the experiments. Aside from these basic components, a variety of auxiliary equipment was employed in the preparatory and terminating stages of a data run and for acquisition of both thermal and melt shape data. A general description of the apparatus will be presented in the subsequent subsections, with further details being available in [9].

Heated vertical cylinder

The heated cylinder consisted of a thick-walled copper sleeve (0.635 cm thick, 2.54 cm in outer diameter and 25.4 cm long) and a brass core (0.32 cm thick and 24.9 cm long). Both the wall thickness of the sleeve and the use of copper were motivated by the desire to obtain a spatially uniform wall temperature at each instant of time during the melting process. As documented and explained later, this objective was not wholly fulfilled in that modest axial temperature variations were encountered, the maximum magnitude of which was 10% of the difference between the mean wall temperature and the melting temperature. Circumferential temperature uniformity was, however, achieved.

The axial temperature differences are sufficiently small so that the results can be regarded as corresponding to the case of spatially uniform wall temperature. The use of a thicker copper wall would have diminished the axial wall temperature variations but at the expense of a higher wall heat capacity, the effect of which would be to intercept and store heat that would otherwise flow into the phase-change medium.

The brass core served to house Teflon-coated electrical resistance wire (30 gage alumel) which was laid in six equally spaced axial grooves which ran the entire length of the core tube. Once the wiring had been completed, the core was soldered to the sleeve, thereby ensuring good thermal contact.

Tube wall temperatures were measured by twelve thermocouples, nine of which were axially distributed along a single vertical line while the other three were deployed along a second vertical line displaced by 180° from the first. To facilitate the installation of the thermocouples, a radial hole was drilled through the tube wall at each thermocouple location. Then, copper plugs, fabricated to the proper dimensions for a press fit into the radial holes, were each equipped with a thermocouple. The plugs were pressed into the holes to a predetermined depth, subsequent to which the outer diameter of the tube was turned and then polished to the desired finished dimension (2.54 cm).

As a result of these operations, the exposed surface of each plug blended perfectly into the remainder of the copper surface, so that the plug locations could not be detected with the naked eye.

The thermocouple junctions were situated 0.076 cm from the exposed surface of the copper sleeve, and the lead wires were threaded through the hollow bore of the core tube and taken out through the bottom of the tube.

To avoid thermal interactions between the heated vertical cylinder and the environment which surrounds the containment vessel, the cylinder was elevated above the floor of the containment vessel. The pedestal which was employed to elevate and support the cylinder was designed to minimize heat conduction between the cylinder and the containment vessel floor while having sufficient strength to bear the load imposed by the cylinder. The pedestal was fabricated from thin-walled stainless steel tubing (0.0254 cm wall thickness, 0.63 cm o.d.) and had a vertical height of 2.86 cm. Its attachment to the base of the heated vertical cylinder and to the floor of the containment vessel are described in [9].

The thermocouple and electric power leads from the heated cylinder were threaded through the bore of the pedestal, from which they were led out of the apparatus. The pedestal itself was equipped with two thermocouples to facilitate estimation of axial heat conduction. Furthermore, to reduce possible extraneous melting, the pedestal was enveloped with an annular section of styrofoam insulation having an outer diameter of 2.54 cm. The outside surfaces of the styrofoam were covered with epoxy to form a barrier to the absorption of molten paraffin.

The minimization of extraneous heat losses was also the motivation for the closure employed at the upper end of the heated cylinder. First, the end face of the copper sleeve was bevelled with a radially inward downslope, so that the inner bevelled edge was axially aligned with the end face of the brass core tube. A thin brass wafer was then placed over the bore of the core tube. The wafer and the bevelled edge of the copper sleeve formed a shallow cavity which was filled with an epoxy (thermal conductivity = 1.49 W/m-C) after attempts to permanently affix a styrofoam cap in the cavity had not been successful. The epoxy, although by no means a very good insulator, has a very much lower thermal conductivity than either brass or copper.

Containment vessel

The containment vessel can be regarded as consisting of two parts—an open-topped cylindrical container and a cover. The cylindrical container was made up of a Plexiglass cylinder 21.6 cm in internal diameter, 0.635 cm thick, and 28.3 cm in height) which was permanently attached to a circular brass plate that served as the base of the container. A number of covers were fabricated to be used either during a data run, during the preparatory stage prior to a data run, or for support of the heater tube assembly when the apparatus was not in use.

The cover used for the runs with a velocity slip boundary condition at the upper surface of the melt region consisted of a hollow, hat-like externally insulated Plexiglass structure. It was designed to provide an air space above the phase-change medium that was thermally isolated from the surroundings. The air space, in addition to allowing for velocity slip, also served to accommodate the additional volume created by the decrease in density which accompanies melting.

For the data runs with a no-slip velocity boundary condition at the upper surface of the melt layer, an annulus of styrofoam insulation, 5.08 cm thick, was housed in the aforementioned hat-like Plexiglass structure. The lower face of the styrofoam, which was coated with a highly polished layer of epoxy, was pressed downward on the upper surface of the phase-change medium by a spring-like arrangement situated atop the styrofoam, thereby imposing the no-slip boundary condition. Four thermocouples installed within the epoxy layer were used to sense the temperatures at the contacting surface of the phase-change medium.

To accommodate the volume change which accompanies phase change, an expansion space was created by positioning a plexiglass tube in the center hole of the styrofoam annulus. The tube is positively positioned by the hat-like structure. The lower end of the tube, the epoxy-coated face of the styrofoam annulus, and the upper end of the heated vertical cylinder all lie in a common horizontal plane. Furthermore, the plexiglass expansion tube and the heated cylinder are concentric, but the 3.18 cm I.D. of the former exceeds the 2.54 O.D. of the latter, thereby leaving 0.32 cm annular gap. It is through this narrow gap that the excess volume of molten paraffin escapes. Three thermocouples were installed in the wall of the expansion tube to monitor the temperatures of the liquid contained therein.

The containment-vessel covers described in the preceding paragraphs were employed during the data runs. In the preparatory stage of each data run, the previously molten paraffin was solidified, and the freezing was performed under vacuum in order to remove air bubbles. Furthermore, owing to the contraction which occurs as the paraffin passes from the liquid to the solid state, it was necessary to add paraffin during the solidification process. A special cover was fabricated which provided an air-tight seal, a connection for attachment of a vacuum pump, and a rapid access port for paraffin addition [9].

The pedestal which supports the heated vertical cylinder from below was of lightweight construction to minimize extraneous heat conduction and, as a consequence, it is fragile. To provide additional support for the heated cylinder, thereby unburdening the pedestal, a containment-vessel cover which provides both positive vertical and radial positioning was fabricated [9]. It was utilized at all times other than

during the actual data runs, the preceding preparatory periods, and the post-run melt shape determinations.

Other apparatus components; instrumentation

To obtain a controlled thermal environment for the containment vessel during both the preparatory stage of each data run and the run itself, the vessel was positioned in a constant-temperature water bath. The bath has a 50 litre capacity, measures $38 \times 51 \times 39$ cm (length $\times$ width $\times$ height), and is made of stainless steel. It is enveloped on all four sides and at the bottom by 10 cm of fiberglass insulation and enclosed in a wooden housing. Flexible plastic sheeting was used to cover the top of the bath to minimize evaporation of water. Temperature control and circulation of the water in the bath was accomplished with a Lauda model B-1 immersion heater/circulator. Spatial and timewise temperature uniformity within the bath corresponding to a given set point was within 0.1°C.

Auxiliary equipment was employed during the freezing of the paraffin—the freezing being one of the key preparatory steps that preceded a data run. The objective of the freezing operation was to obtain a homogeneous void-free solid. As was mentioned earlier, air bubbles were effectively eliminated by freezing under vacuum (the vacuum was about 640 mm Hg).

Of even greater concern is the possible occurrence of voids associated with the contraction which accompanies freezing. Void formation was prevented by a freezing pattern which proceeds from the bottom upward. To ensure the attainment of this freezing pattern, chilled water from a temperature controlled refrigeration unit was passed through coiled copper tubing soldered to the underside of the brass-base plate of the containment vessel. In addition, an intensity-controlled radiant lamp suspended above the containment vessel prevented the formation of a frozen skin at the top of the vessel during the freezing process.

Another auxiliary device associated with the freezing operation was a 25.4 cm length of straight copper tubing heated by circulating hot water. This tube was employed immediately after the completion of freezing to finish off the exposed upper surface of the solidified paraffin. The objective of the finishing procedure was to obtain a flat upper surface whose level is coincident with the exposed tip of the vertical test cylinder.

For those cases in which the solid phase-change material was at a temperature below the fusion temperature at the beginning of the data run, it was deemed desirable to deploy thermocouples in the solid in order to chart the temperature field which is created by the heating of the test cylinder. The thermocouples were installed in the phase-change medium when it was in the liquid state, prior to the initiation of the freezing operation. Positive positioning of the thermocouple junctions was accomplished by threading the lead wires through a template situated at the top of the containment vessel and by small lead weights suspended from the respective junctions by 25 μm nylon thread. All told, nine such thermocouples were installed, one set of which was radially distributed at a depth of 2.54 cm below the top of the vessel while a second set was placed at a depth of 12.7 cm.

At the termination of each data run, it was found advantageous to immediately remove the liquid melt from the containment vessel. This was accomplished by a vacuum system which deposited the liquid in a stainless-steel canister.

Attention will now be turned to the instrumentation and to the electrical equipment.

All thermocouples were made of specially calibrated, Teflon-coated chromel and alumel wire. The thermocouples situated in the subcooled solid were of 36 gage wire, while all other thermocouples were of 30 gage wire. The transient nature of the experiments required that the thermocouples be read and recorded rapidly, especially at the beginning of the data run. A Doric Digitrend 210 datalogger with a 1 μV resolution was employed for reading and recording the thermocouple data.

Electric power was supplied to the resistance wire in the vertical heated cylinder by a regulated d.c. supply. Both the voltage drop across the heater wire and the current flow were read with five-digit d.c. voltmeters (the current flow was measured across a calibrated shunt).

The measurement of the shape of the melt cavity was accomplished by highly precise feeler gages. As will be seen later, the outer bounding surface of the cavity (i.e. the surface of the unmelted solid) has a shape similar to an inverted bell—that is, the wide portion is at the top. For the lower portion of the cavity, where the outer bounding wall departs only moderately from the vertical, a feeler gage was employed which measures the radial gap between the walls of the cavity. On the other hand, adjacent to the top of the cavity, the outer bounding surface tends toward the horizontal and a depth gage was employed. These gages and their use are described more fully in [9].

Experimental procedure

Many of the key details of the experimental procedure have been described in the preceding subsections of the paper. Here, an overview will be presented in order to tie together the various steps in the execution of a data run.

At the conclusion of a data run, most of the containment vessel was occupied by solid paraffin (at most, the melt cavity occupied about 10% of the volume of the vessel). With a view to obtaining, for the next melting experiment, a solid phase which is homogeneous throughout the entire containment vessel, the aforementioned residual solid was liquefied and then solidified, with additional liquid paraffin being added as needed to completely fill the vessel.

Subsequent to the solidification of the paraffin, which required about 36 h for completion, an equilibration period was initiated during which the contents of the containment vessel approached and ultimately

attained a uniform temperature equal to that of the water bath in which the vessel was situated. The bath temperature was set so that either of two equilibrium temperatures would be attained by the solid paraffin—either the melting point value (36.4°C) or a lower than melting value of 22°C, representing a subcooling of 14.4°C. In actuality, for the first of these cases, it was found desirable to subcool by a few tenths of a degree below the melting temperature to avoid melting of the impurities (the paraffin used in the experiments was 99% pure *n*-eicosane). The attainment of thermal equilibrium in the solid required about 72 h.

A data run was initiated by the application of electric power to the core of the vertical heated tube. During the rapid initial transient that followed the onset of heating, temperature data were recorded continuously at the rate of two channels per second. Subsequently, data were collected every minute, and as the variations became more and more gradual, measurement intervals of 5, 10, 20, and 30 min were used, depending on the duration of the run. Run times ranged from 75 min to $17\frac{1}{2}$ h, and the run times were correlated with the corresponding power inputs so that the product of run time and power (i.e. energy input) was the same at the termination of each run. The containment vessel was situated in the water bath during the entire duration of the run, and the bath temperature was maintained at a value equal to the temperature of the solid at the onset of heating.

At the termination of a data run, the heater power was turned off and the molten paraffin drawn from the melt cavity using the vacuum system that was described earlier. Once this had been accomplished, the containment vessel was removed from the water bath and placed on a bench, where the melt shape contours were measured.

DATA REDUCTION

The procedures used to deduce transient and steady-state heat transfer coefficients from the measured heated-tube temperatures and power inputs will now be described. In addition, the dimensionless parameters employed in the correlation of the steady-state heat transfer coefficients will be set forth and rationalized.

The heat transfer coefficients to be determined here are instantaneous spatial-average values defined by

$$h(t) = Q(t)/A[\bar{T}_w(t) - T^*] \tag{1}$$

where the time-dependence has been indicated explicitly. In equation (1), Q denotes the instantaneous rate of heat transfer from the heated cylinder to the phase-change medium, A is the area of the cylindrical surface, $\bar{T}_w$ is the spatially averaged surface temperature of the cylinder, and T^* is the melting temperature.

Attention will first be given to the determination of $\bar{T}_w(t)$. In this regard, note should be taken of the fact that the twelve thermocouples embedded in the cylinder wall were read successively over a time span of about 0.1 min. Therefore, the various measured temperatures did not correspond to precisely the same time t. With regard to the averaging of the individual wall temperatures to get $\bar{T}_w(t)$, the existence of the 0.1 min span is of practical importance only during the rapid initial transient, not only in its effect on $[\bar{T}_w(t) - T^*]$ but also in its error-causing potential in the evaluation of $\mathrm{d}\bar{T}_w/\mathrm{d}t$, whose significance will be explained shortly.

To deal with this situation, an interpolation algorithm was employed to evaluate the temperatures at certain preselected times for all the thermocouple stations on the cylinder wall. The preselected times corresponded to 1 min intervals, and the temperature data used in the interpolation were those for times immediately adjacent to the preselected values. The interpolation formula was self checking and used that number of terms to obtain an accuracy of 0.03°C.

In view of the observed circumferential uniformity, only the nine thermocouples lying along the main vertical line of installed thermocouples were employed in the averaging process to obtain $\bar{T}_w(t)$. Both unweighted averaging and surface-area-weighted averaging were investigated, but the differences were within the accuracy of the measurements. As noted earlier, the overall spatial variation of T_w at any instant of time did not exceed 10% of $(\bar{T}_w - T^*)$.

With regard to the heat transfer rate $Q(t)$, the electric power input to the embedded heater was measured at 1 min intervals during the period of rapid transients and at larger intervals thereafter. Owing to the heat capacity of the copper and brass which constituted the heated cylinder, a portion of the electric power input was intercepted and stored in these metallic elements, especially during the early stages of a data run when the rate of change of the tube wall temperature with time was rapid.

If account is taken of this storage, to be denoted by $S(t)$, and of the fact that extraneous losses from the heated tube are negligible (Appendix C of [9]), then

$$Q(t) = P(t) - S(t). \tag{2}$$

The electric power P is very nearly constant (slight changes occurred owing to the change of heater resistance with temperature), while the storage term was evaluated from

$$S(t) = C(\mathrm{d}\bar{T}_w/\mathrm{d}t) \tag{3}$$

where C is the heat capacity of the wall of the heated cylinder. The derivative in equation (3) was evaluated by central differences.

Appreciable deviations of $Q(t)$ from $P(t)$ occurred only during the initial period of any given data run. For the high-power, short-duration runs (power densities from 1530 to 3060 W/m^2, run times from 150 to 75 min), deviations were in evidence for about the first 15% of the duration time of the run when there was no subcooling and for about the first 20% for the subcooling runs. With decreasing power and longer

duration runs, the period when $S(t)$ played an important role diminished markedly to a lesser percentage of the run time.

The heat transfer coefficients were found to attain a steady value after a sufficient period of time, and a dimensionless correlation of these steady-state results was sought using the Nusselt and Rayleigh numbers, defined as

$$Nu = hL_c/k, \quad Ra = [g\beta(\bar{T}_w - T^*)L_c^3/\nu^2](c_p\mu/k) \tag{4}$$

in which L_c is a characteristic length, and $(\bar{T}_w - T^*)$ is the steady-state temperature difference. The thermophysical properties of the molten paraffin were taken from [10] and were evaluated at the mean of $\bar{T}_w$ and T^*.

Two characteristic lengths were used in the correlation effort. One of these was the length L of the cylinder. The other characteristic length was motivated by the standard practice used in correlations of natural convection heat transfer coefficients in enclosed layers, where the horizontal thickness of the layer is employed as the length dimension. In the present instance, the thickness of the natural convection layer (i.e. the melt layer) is a variable and is also an unknown with respect to a potential user of a correlation. In view of this, a global, user-oriented approach to evaluating a layer thickness L^* was formulated as follows.

First, let $E(t)$ denote the energy input to the phase-change medium between times $t = 0$ and $t = t$. If sensible heat effects in the molten material are neglected, then the melt cavity volume is $E/\rho\lambda$ (ρ = liquid density, λ = latent heat per unit mass), and an effective cross-sectional area can be written as $(E/\rho\lambda)/L$, where L is the length of the cylinder. If the outer radius of the effective cross section is r^* and its thickness is L^*, then

$$\pi(r^{*2} - r_0^2) = E/\rho\lambda L, \quad L^* = r^* - r_0. \tag{5}$$

It is also convenient to define a dimensionless time

$$\tau = E(t)/\rho\lambda\pi r_0^2 L \tag{6}$$

so that, from equations (5) and (6)

$$L^* = r_0[(\tau + 1)^{1/2} - 1]. \tag{7}$$

As is easily verified, L^* can be evaluated from equation (7) by introducing readily available information into the right-hand side.

The actual dimensionless correlations will be developed in the next section of the paper.

RESULTS AND DISCUSSION

The presentation of results will begin with the temperature history of the heated tube and then goes on to the quantitative heat transfer results for both the transient and steady-state regimes. These results encompass both the open-top and closed-top configurations and the subcooled and non-subcooled states of the solid. Representative melt region shapes are presented to round out the results.

Temperature history of heated cylinder

The history of the cylinder wall temperature provides information and insights about the physical processes which occur during melting and, in the case of initial subcooling, during the pre-melting stage. Representative wall temperatures are presented in Figs. 1 and 2 without initial subcooling and with initial subcooling, respectively. In each figure, results are given for two heater input power densities (based on the surface area of the cylinder) equal to 510 and 3060 W/m^2. These power densities typify the upper and lower ends of the range employed in the present experiments. The figures correspond to the closed-top case (no-slip boundary condition for the velocity), but, as will be demonstrated shortly, neither the qualitative nor the quantitative heat transfer results are affected by the velocity condition at the upper bounding surface.

For each case dealt with in the figures, the temperature at each of three selected axial stations, characterized by the coordinate x measured downward from the top of the heated cylinder, is plotted as a function of time. As noted earlier, temperatures were measured at nine axial stations, but the presentation of results at more than three stations would have led to a highly cluttered graph.

Attention is first directed to Fig. 1 (without subcooling). As seen there, the initial rapid rise of the wall temperature soon gives way to a more gradual rise which, in turn, leads to the attainment of a maximum and a subsequent slow decrease to a steady value. During the initial rise, spatial uniformity prevails. Axial variations become evident as the temperature increase slows and attain prominence as the maximum is approached. These variations are such that the temperature is lowest at the bottom of the cylinder and increases along the height of the cylinder.

The absence of axial variations during the initial stage of the transient reinforces the notion that radial conduction across the melt layer is the sole mode of heat transfer in the period immediately following the onset of heating. During this period, the thickness of the melt layer at any given time is uniform along the height of the cylinder. As the melt layer grows thicker, buoyancy forces created by the radial temperature variation across the layer are able to overcome the frictional resistance and, thereby, to initiate a recirculating motion—upward adjacent to the cylinder and downward adjacent to the melting interface.

This motion is weak at first, so that conduction continues to play a role. However, as the natural convection grows stronger and dominates conduction, it works to reduce the thermal resistance for heat transfer between the cylinder and the melting interface. This reduction in thermal resistance is responsible for the observed maximum in the temperature–time curves of Fig. 1 and for the subsequent dropoff.

The occurrence of steady values of the wall temperature at larger times is worthy of note, especially since the melt cavity continues to grow. This behavior is consistent with a model whereby the thermal resistance between the cylinder and the melting interface is dominated by that at the cylinder surface, with the resistance at the interface being very small because of the relatively large surface area of the interface. Thus, the overall resistance is independent of what is happening at the interface and thereby becomes independent of time. Since the cylinder heat flux is also independent of time after the initial portion of the heating period, the temporal constancy of the wall temperature follows directly.

The axial temperature variation in evidence in Fig. 1 is a direct consequence of the decrease of the natural convection heat transfer coefficient along the height of the tube. During the design of the apparatus, it was expected that the use of a thick-walled copper cylinder would neutralize the effects of the expected axial variation of the transfer coefficient. When this was found not to be the case, finite-difference heat conduction calculations for the cylinder wall were undertaken [9]. Input values of the natural convection heat transfer coefficient were obtained by assuming a linear decrease of the coefficient along the height of the cylinder, with the spatial mean coefficient being equal to the experimentally determined value.

These calculations showed that a factor of two decrease in the coefficient from the bottom to the top of the cylinder is sufficient to account for the observed axial temperature variations. A thicker cylinder wall would have reduced the temperature variations, but this would have been accomplished at the cost of an increased wall heat capacity.

The wall temperature results for the case of initial subcooling will now be considered (Fig. 2). These

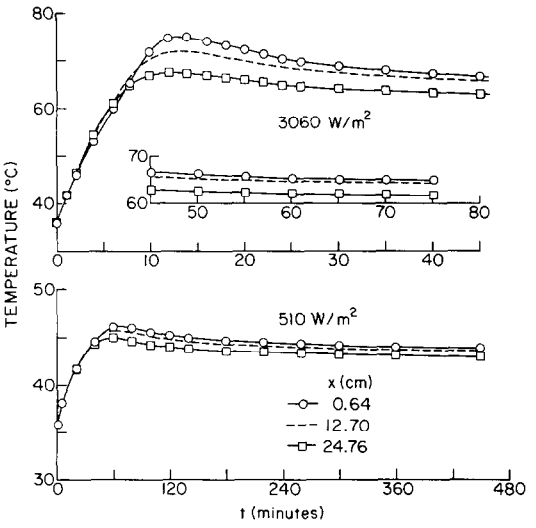

FIG. 1. Temperature history of the wall of the heated cylinder for input power densities of 510 and 3060 W/m²; closed-top case, no initial subcooling.

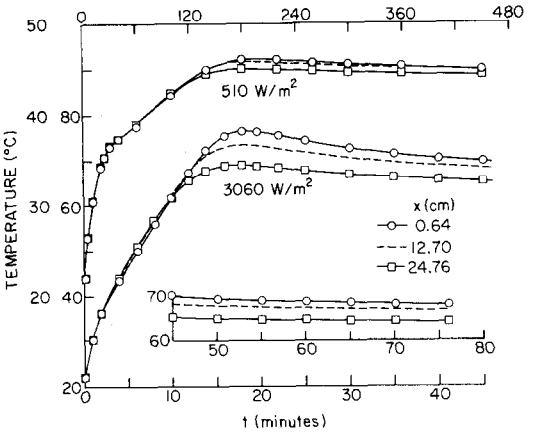

FIG. 2. Temperature history of the wall of the heated cylinder for input power densities of 510 and 3060 W/m²; closed-top case, initial subcooling = 14.4°C.

results are similar to those already discussed for the no-subcooling case, except for the period which follows the onset of heating. During this period, heat flows radially outward from the cylinder to the subcooled solid, and there is no melting until the wall temperature reaches 36.4°C. At that point, the onset of melting is marked by a sharp change in the slope of the temperature–time curves.

Instantaneous heat transfer coefficients

Timewise variations of the spatial-average cylinder heat transfer coefficient are presented in Figs. 3 and 4 for the no-subcooling case. These figures correspond respectively to the no-slip and slip velocity boundary conditions at the upper surface of the paraffin, i.e. the closed and open tops. Instead of using the actual time as the abscissa, a more general presentation has been achieved in terms of the dimensionless time τ of equation (6), in which $E(t)$ represents the energy input to the phase-change medium between $t = 0$ and $t = t$.

Inspection of Figs. 3 and 4 reveals a pattern that is

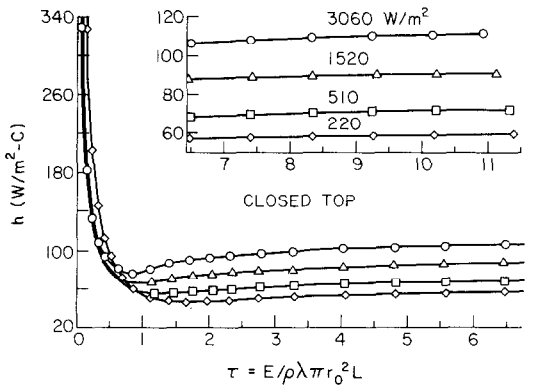

FIG. 3. Timewise variations of the cylinder heat transfer coefficient for the closed-top case and no subcooling.

common to all the curves. Starting with very high values at early times, the heat transfer coefficient decreases, sharply at first and then gradually, attains a minimum and increases gradually to a steady-state value. The h vs τ distributions of Figs. 3 and 4 are reciprocal to the temperature–time distributions of Figs. 1 and 2, which is consistent with the fact that the rate of heat transfer from the cylinder to the phase-change medium is constant over most of the heating period. On the basis of the discussion presented in connection with Figs. 1 and 2, various regimes—conduction, onset of convection, dominance of convection, steady state—can be identified in Figs. 3 and 4.

In the convection regime, higher heat transfer coefficients are in evidence at higher values of the input power. This finding is readily rationalized by noting that higher input powers give rise to larger temperature differences between the cylinder wall and the interface, thereby producing a greater buoyancy force and a more vigorous natural convection. The variation of the steady-state heat transfer coefficient with input power will shortly be correlated in terms of the Nusselt and Rayleigh numbers.

It is of practical interest to provide a means of estimating the time at which the steady-state regime sets in. Since the approach to steady state is gradual, it is reasonable to define τ_{ss} as the τ value at which h has attained 95% of its steady-state value. Whereas τ_{ss} varies slightly with the power level and with the top-surface velocity condition, a value $\tau_{ss} \simeq 5$ provides an adequate estimate for all cases.

As a final observation with respect to Figs. 3 and 4, it may be noted that the minima of the respective curves are displaced to higher τ values at lower power inputs. The minimum can be regarded as the point at which natural convection begins to overpower the radial heat conduction in the melt layer. At lower power inputs, the cylinder-to-interface temperature difference is smaller, and a thicker melt layer is needed to enable the natural convection to attain the same degree of vigor as at higher input powers. Since τ [via $E(t)$] is a measure of the thickness of the melt layer, the larger τ values which mark the minimum point at lower powers appear reasonable.

One of the major objectives of the present research is to assess how the cylinder heat transfer coefficients are affected by the velocity boundary condition at the upper surface of the phase-change medium. This issue is addressed in Fig. 5, where the results for the closed-top and open-top cases (no slip and slip) are compared at the highest and lowest power inputs investigated. The figure shows that the heat transfer coefficients for the two types of boundary conditions are in complete agreement, within the resolving power of the experiments. Thus, at least for the no-subcooling case, the cylinder heat transfer coefficients are unaffected by the upper-surface velocity boundary condition. From the standpoint of practice, this is a convenient result since it eliminates the necessity of using different heat transfer coefficients for the two types of velocity boundary conditions.

A presentation of instantaneous heat transfer coefficients for the subcooling case (14.4°C below the melting temperature) is made in Figs. 6–8 using a format that is identical to that used in Figs. 3–5 for the no-subcooling case. Figures 6 and 7 convey results for the closed top and the open top, respectively, while Fig. 8 presents a comparison of results for the two types of top configurations.

From an overview, it is seen that all of the main trends that were identified in Figs. 3 and 4 for no-subcooling are in evidence in Figs. 5 and 6 for subcooling, and the previously discussed ramifications and rationalizations continue to apply. However, Figs. 5 and 6 contain a unique feature, namely, a strong input-power-related rightward shift of the curves in the range of small times. This shift can be traced to the fact that, beginning at a given subcooled state, larger energy inputs E are required to bring the cylinder temperature up to the melting temperature (i.e. 36.4°C) at lower power levels than at higher power levels. The need for the larger energy input is correlated with the slower rates of temperature rise at lower power levels,

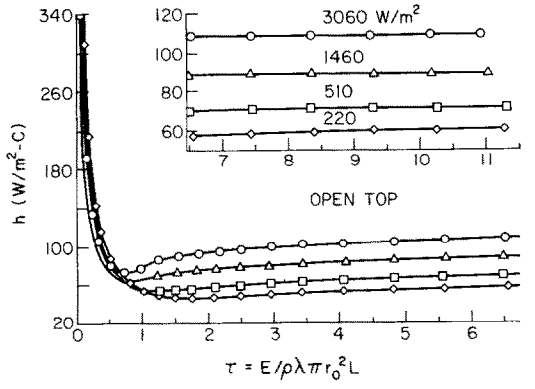

FIG. 4. Timewise variations of the cylinder heat transfer coefficient for the open-top case and no subcooling.

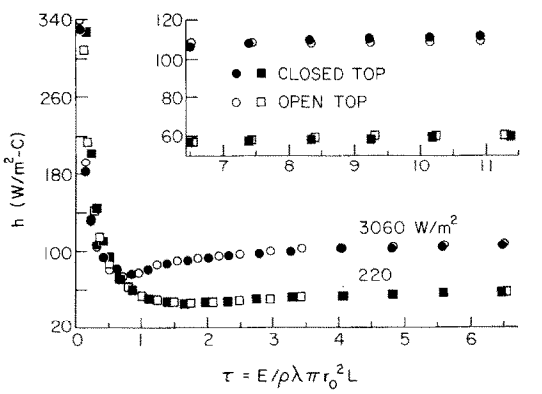

FIG. 5. Comparison of heat transfer results for the closed-top and open-top cases; no subcooling.

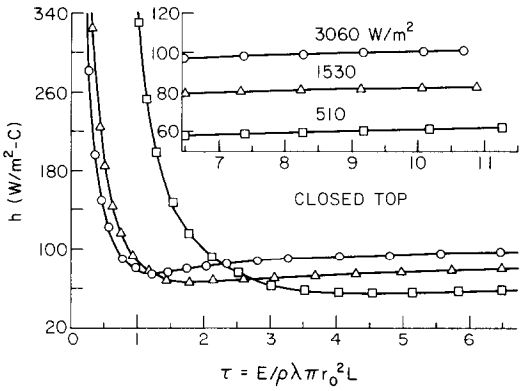

FIG. 6. Timewise variations of the cylinder heat transfer coefficient for the closed-top case; initial subcooling = 14.4°C.

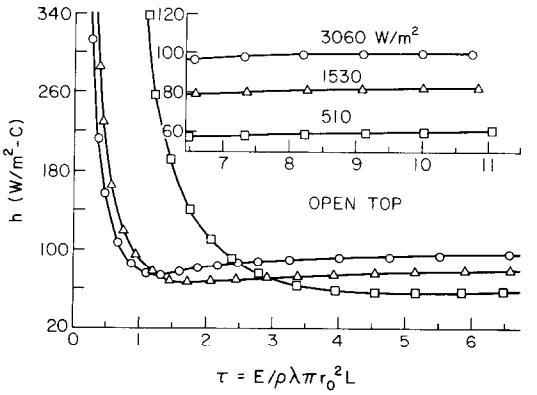

FIG. 7. Timewise variations of the cylinder heat transfer coefficient for the open-top case; initial subcooling = 14.4°C.

so that there is more time for heat to diffuse from the cylinder surface to more remote parts of the subcooled solid.

The τ values ($= \tau_m$) at the onset of melting are, therefore, larger at lower powers. Furthermore, for $\tau < \tau_m$, h is negative since $T_w < T^*$, and at $\tau = \tau_m$, $h = \infty$. Thus, there is a range of τ values where the curves for higher powers indicate positive values of h and are descending, while those for smaller powers are still reflecting negative h values (not shown in Figs. 6 and 7), i.e. the crossover from negative h to large positive h occurs at larger τ for small power levels. These characteristics make plausible the early-time rightward shift in evidence in Figs. 6 and 7.

Figures 6 and 7 also enable the identification of a dimensionless time τ_{ss} at which the steady state is, in effect, attained (i.e. h values within 5% of the steady values). A value of $\tau_{ss} \simeq 6.5$ appears to be suitable for all the cases dealt with in the figures. This τ_{ss} value is larger than that previously identified for no subcooling, which is not surprising since $E(t)$ appearing in τ now includes the energy required to overcome the initial subcooling.

A comparison of results for the closed- and open-top configurations in the presence of subcooling is made in Fig. 8 for two input powers which typify the high and low ends of the range. The virtual coincidence of the open and blackened data symbols leads to the conclusion that the heat transfer coefficients at the heated cylinder are unaffected by the upper-surface velocity condition, both for no subcooling and for subcooling.

An issue which was of some concern in the longer subcooled-solid data runs relates to whether the temperature wave which moves radially outward through the solid interacts strongly with the wall of the containment vessel. Such a strong interaction might have affected the measured heat transfer coefficients (i.e. those of Figs. 6–8). Finite-difference computations undertaken to examine this issue (Appendix B of [9]) indicated that the interaction had a negligible effect on the coefficients.

To conclude the presentation of the instantaneous heat transfer coefficients, a comparison will be made between the results with and without subcooling. The comparison, which is presented in Fig. 9, is based on data for the closed-top case, but an identical comparison holds for the open-top case.

Examination of Fig. 9 reveals two major differences

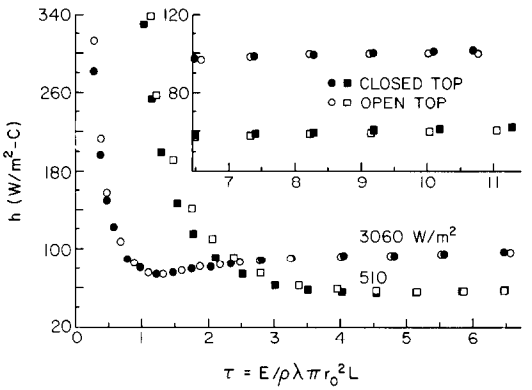

FIG. 8. Comparison of heat transfer results for the closed-top and open-top cases; initial subcooling = 14.4°C.

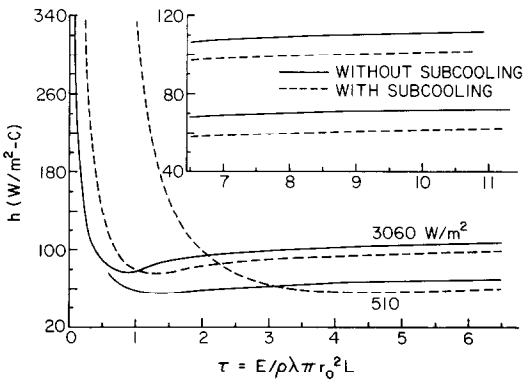

FIG. 9. Comparison of heat transfer results with and without subcooling; closed-top case.

between the results with and without subcooling. The first is the rightward shifting of the subcooling curves at small values of time. This shifting has already been rationalized and need not be discussed further. The other, more novel difference is that in the convection-dominated regime, the heat transfer coefficients in the presence of subcooling are always lower than those without subcooling, the deviations being in the 10–15% range. This finding is especially interesting because the opposite ordering would occur if conduction were the sole mode of heat transfer. The primacy of the no-subcooling coefficients in the presence of convection can be understood by noting that the size of the melt cavity is smaller when there is subcooling than when subcooling is absent. The smaller melt cavity diminishes the vigor of the natural convection motions which, in turn, reduces the heat transfer coefficients.

Steady-state Nusselt numbers

The steady-state heat transfer coefficients exhibited in the various preceding figures, supplemented by others from data runs not yet reported, have been cast in dimensionless form according to the definitions of equation (4). For the first of the correlations of the data, the cylinder length L will be used as the characteristic dimension, and the corresponding Nusselt and Rayleigh numbers are designated as Nu_L and Ra_L. The steady-state data are plotted in terms of these parameters in Fig. 10.

As seen in the figure, the results for the no-subcooling and subcooling cases fall along the separate least-squares lines, which are respectively represented by

$$Nu_L = 0.393Re_L^{0.267}, \quad Nu_L = 0.096Re_L^{0.323} \tag{8}$$

with no effect in evidence of the velocity condition at the upper surface of the phase-change medium. Also shown is an extrapolation of analytical predictions by Hossfeld [8] for no subcooling and for a closed top.

In [8], Nu_L was plotted as a function of time for Ra_L values of 2.9×10^6 and 7×10^8. We have inferred a steady-state value for each of these cases, and a power-law relation $Nu_L = 0.182Ra_L^{0.308}$ was passed through the two steady-state points. This relation is represented by the dashed line in Fig. 10. The agreement between the dashed line and the present no-subcooling data is within 10% or better. This level of agreement has to be regarded as highly satisfactory, especially considering the aforementioned extrapolations.

For natural convection in parallel-walled vertical enclosures (without phase change), it is common to use the gap width between the walls as the characteristic length. To explore how the present steady-state results relate to literature information for natural convection in parallel-walled enclosures, the Nu_L, Ra_L correlations of equation (8) will be recast into Nu_{L*}, Ra_{L*} correlations, where L^* is the effective gap width defined by equation (7). This gives

$$Nu_{L*} = 0.393Ra_{L*}^{0.267}(AR)^{-0.199} \tag{9}$$

$$Nu_{L*} = 0.096Ra_{L*}^{0.323}(AR)^{-0.030} \tag{10}$$

respectively for no subcooling and subcooling, where AR represents the aspect ratio

$$AR = L/L^*. \tag{11}$$

From an examination of the literature encompassing both analysis and experiments on natural convection in vertical parallel-walled enclosures [9], a range of exponents for both Ra and AR was encountered. The exponent of Ra varied from 0.263 to 0.315, while the exponent of AR ranged from -0.131 to -0.300. The present exponents for no subcooling, 0.267 and -0.199 respectively, fall squarely in the literature ranges. This is a highly affirmative finding since the present melt cavities do not have parallel walls. The subcooling results, equation (10), do not agree well with those of the natural convection literature. These deviations may be attributed to the inhibitions imposed on the natural convection due to the narrowness of the gap in the lower part of the melt cavity when subcooling is present.

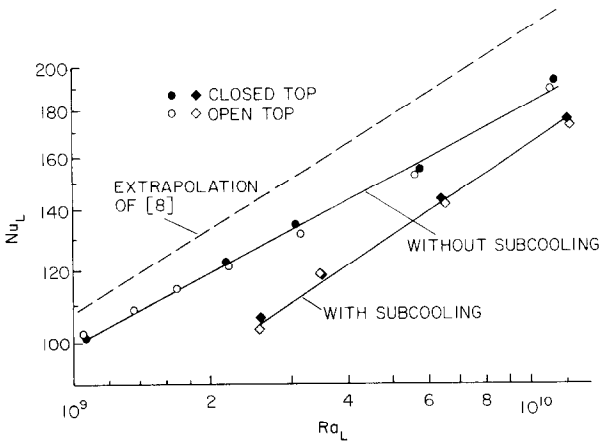

FIG. 10. Nusselt–Rayleigh representation for the steady-state heat transfer coefficients.

Melt cavity shapes

Representative shapes of the melt cavity are presented in Fig. 11, with a fuller presentation available in [9]. Figure 11 conveys results for a power level of 3060 W/m², with (a) and (b) parts for no subcooling and subcooling, respectively. The energy input to the phase-change medium is identical for all the cases exhibited in the figure. In general, the melt cavities have a similar shape for all cases, being widest at the top and tapering down to a relatively narrow thickness near the bottom. This shape is consistent with a natural convection recirculation that is upward along the heated cylinder and downward along the liquid–solid interface.

Referring to the (a) part of the figure, it is seen that the open-top boundary condition enables the development of a much flatter profile in the upper portion of the cavity than does the closed-top boundary condition. Then, upon comparing the (a) and (b) parts of the figure, the diminution of the melt cavity size due to subcooling is clearly in evidence.

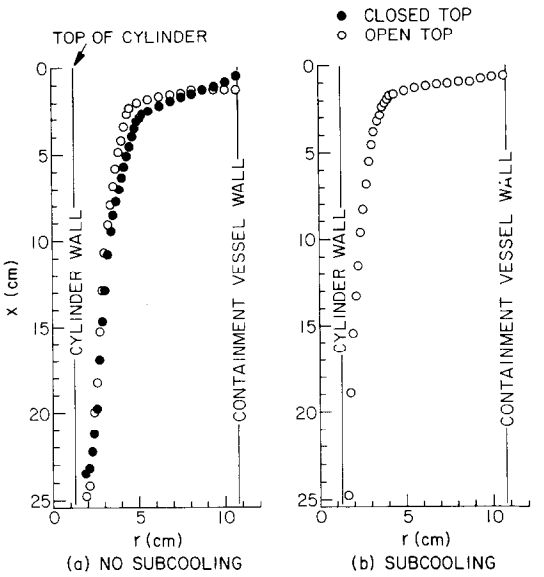

FIG. 11. Representative melt cavity shapes; input power density = 3060 W/m², same energy input for all cases.

CONCLUDING REMARKS

These experiments have provided quantitative heat transfer data for melting about a heated vertical cylinder embedded in a phase-change medium. In addition, the initial, short-lived dominance of heat conduction in the melt layer and the subsequent primacy of natural convection was identified via instantaneous cylinder wall temperature distributions and heat transfer coefficients and by melt cavity profiles.

It was found that the heat transfer coefficients are not affected by whether the upper surface of the phase-change medium is closed by a cover which imposes a no-slip velocity boundary condition or is bounded by an insulated air space which permits motion of the liquid melt. This finding is applicable to both the melting of a non-subcooled solid or a subcooled solid. Subcooling tends to delay the onset of natural convection dominance. The natural convection heat transfer coefficients in the presence of subcooling are 10–15% lower than those for the non-subcooled case.

A steady state characterized by time-independent heat transfer coefficients was encountered at sufficiently large times after the onset of heating, and a quantitative criterion was established for the onset of the steady regime. The steady-state coefficients were well correlated in terms of the Nusselt and Rayleigh numbers. The functional dependence of the steady-state Nusselt numbers for no subcooling agreed well with the literature for natural convection in vertical, parallel-walled enclosures without melting.

The melt cavities have an inverted bell shape—wide at the top and narrow at the bottom. Subcooling markedly reduces the size of the melt cavity.

Acknowledgement—This research was performed under the auspices of the U.S. Department of Energy, Office of Basic Energy Sciences. The design suggestions of Professor J. W. Ramsey are gratefully acknowledged.

REFERENCES

1. R. Viskanta, A. G. Bathelt and N. W. Hale, Jr., Latent heat-of-fusion energy storage: experiments on heat transfer during solid–liquid phase change, *Proceedings, Third Miami International Conference on Alternative Energy Sources*, (December 1980).
2. R. L. Bain, F. J. Stermole and J. O. Golden, Liquification dynamics of *n*-octadecane in cylindrical coordinates, *J. Spacecraft Rockets* **11**, 335–339 (1974).
3. J. W. Ramsey and E. M. Sparrow, Melting and natural convection due to a vertical embedded heater, *J. Heat Transfer* **100**, 369–370 (1978).
4. N. W. Hale, Jr. and R. Viskanta, Photographic observation of the solid–liquid interface motion during melting of a solid heated from an isothermal vertical wall, *Lett. Heat Mass Transfer* **5**, 329–337 (1978).
5. P. D. Van Buren and R. Viskanta, Interferometric measurement of heat transfer during melting from a vertical surface, *Int. J. Heat Mass Transfer* **23**, 568–571 (1980).
6. M. Bareiss and H. Beer, Influence of natural convection on the melting process in a vertical cylindrical enclosure. *Lett. Heat Mass Transfer* **7**, 329–338 (1980).
7. E. M. Sparrow, S. V. Patankar and S. Ramadhyani, Analysis of melting in the presence of natural convection in the melt region, *J. Heat Transfer* **99**, 521–526 (1977).
8. L. M. Hossfeld, A coordinate transformation method for solving a convection phase change problem, Ph.D. Thesis, Department of Mechanical Engineering, University of Minnesota, Minneapolis, Minnesota (1979).
9. R. G. Kemink, Melting of a solid adjacent to a heated vertical cylinder with or without subcooling of the solid, Ph.D. Thesis, Department of Mechanical Engineering, University of Minnesota, Minneapolis, Minnesota (1981).
10. E. I. Griggs and W. R. Humphries, A design handbook for phase change thermal control and energy storage devices, NASA Technical Paper 1074 (1977).

COEFFICIENTS DE TRANSFERT THERMIQUE POUR LA FUSION AUTOUR D'UN CYLINDRE VERTICAL AVEC OU SANS SOUS-REFROIDISSEMENT ET UN ESPACE OUVERT OU CLOS

Résumé—Des expériences sont conduites pour mesurer les coefficients de transfert thermique lors de la fusion autour d'un cylindre vertical chauffé et noyé dans un milieu solide qui change de phase et dont la température est soit celle de fusion, soit inférieure. La surface supérieure est une couverture solide qui impose une condition aux limites de non-glissement sur le liquide fondu, ou bien un espace d'air qui permet le mouvement sans contrainte du liquide. On mesure aussi la forme de la région fondue. Toutes les expériences sont effectuées avec une paraffine *n*-eicosane pure à 99 pour cent (température de fusion = 36,4°C) et concernent à la fois les périodes transitoires et de régime permanent. Le rapport hauteur/diamètre du cylindre est égal à dix. On trouve que les coefficients de transfert thermique sont identiques pour les configurations à sommet clos ou ouvert. Le sous-refroidissement tend à retarder la prédominence de la convection naturelle. Les coefficients de convection naturelle en présence du sous-refroidissement sont environ 10 à 15 pour cent inférieurs à ceux du cas sans sous-refroidissement. En général, les coefficients de transfert par convection naturelle en régime permanent sont bien unifiés en utilisant les nombres de Nusselt et de Rayleigh et, en l'absence du sous-refroidissement, la dépendance fonctionnelle est semblable à cell de la convection naturelle dans des cavités verticales et parallèles sans fusion.

WÄRMEÜBERGANGSKOEFFIZIENTEN FÜR DEN SCHMELZVORGANG UM EINEN VERTIKALEN ZYLINDER MIT UND OHNE UNTERKÜHLUNG FÜR EINEN OFFENEN UND GESCHLOSSENEN BEHÄLTER

Zusammenfassung—Es wurden Versuche durchgeführt, um die Wärmeübergangskoeffizienten für den Schmelzvorgang um einen beheizten vertikalen Zylinder in einem festen Phasenwechselmedium zu messen, dessen Temperatur entweder am Schmelzpunkt oder etwas darunter lag. Bei den Versuchen war die Oberfläche des Phasenwechselmediums entweder mit einer Abdeckung versehen, an der für die Geschwindigkeit der flüssigen Schmelze die Haftbedingung gilt, oder sie war durch einen isolierten Luftraum begrenzt, der eine unbehinderte Flüssigkeitsbewegung zuließ. Die Form des Schmelzgebietes wurde bestimmt. Bei allen stationären und instationären Versuchen wurde Eicosan–Paraffin (Schmelzpunkt = 36, 4°C) mit einer Reinheit von 99% verwendet. Das Verhältnis von Höhe zu Durchmesser des Zylinders war 10. Es stellte sich heraus, daß die Wärmeübergangskoeffizienten für die oben geschlossene und offene Anordnung identisch sind. Die Unterkühlung führt zur Verzögerung des dominierenden Einflusses der freien Konvektion auf den Wärmeübergangsvorgang. Die Wärmeübergangskoeffizienten der freien Konvektion bei Unterkühlung sind um 10–15% niedriger als diejenigen im nichtunterkühlten Fall. Im allgemeinen ließen sich die stationären Wärmeübergangskoeffizienten bei freier Konvektion gut durch Nusselt- und Rayleigh Zahlen beschreiben, und für den Fall ohne Unterkühlung ergab sich die funktionale Abhängigkeit ähnlich wie bei freier Konvektion in senkrechten Hohlräumen mit parallelen Wänden ohne Schmelzen.

КОЭФФИЦИЕНТЫ ТЕПЛОПЕРЕНОСА ПРИ ПЛАВЛЕНИИ ВЕЩЕСТВА С НЕДОГРЕВОМ ИЛИ БЕЗ НЕГО ВОКРУГ ВЕРТИКАЛЬНОГО ЦИЛИНДРА, ПОМЕЩЕННОГО В ОТКРЫТУЮ ИЛИ ЗАКРЫТУЮ ЕМКОСТЬ

Аннотация — Проведено экспериментальное измерение коэффициентов теплопереноса при плавлении окружающего нагреваемый вертикальный цилиндр твердого вещества, температура которого доводилась до или ниже точки плавления. Если емкость, в которую помещалось вещество, была сверху закрыта крышкой, на жидком расплаве создавалось граничное условие с нулевой скоростью, в то время как в открытой емкости изолирующая прослойка воздуха давала возможность расплаву перемещаться неограниченно. Измерялся профиль области расплава. Все опыты проводились с *n*-эйкозановым парафином чистотой 99% (температура плавления = 36,4°C) в переходном и стационарном режимах. Отношение высоты цилиндра к диаметру равнялось 10. Найдено, что коэффициенты теплопереноса в обеих емкостях идентичны. При недогреве естественная конвекция не сразу играет доминирующую роль в процессе теплообмена. В этом случае коэффициенты теплопереноса примерно на 10–15% ниже значений, полученных без недогрева. В общем случае коэффициенты теплопереноса в стационарных условиях естественной конвекции хорошо описываются зависимостью Нуссельта от Релея. Показано, что при нагревании вещества полученная функциональная зависимость аналогична соотношению, описывающему процесс естественной конвекции в вертикальных каналах с параллельными стенками без плавления.